Sequential thermomechanical analysis of a laser powder bed fusion build

This example illustrates the sequential thermomechanical analysis of a laser powder bed fusion three-dimensional build of a bridge structure. The model in this problem is created based on the AMB2018-01 Additive Manufacturing benchmark problem published by the National Institute of Standards and Technology (NIST). A transient heat transfer analysis is performed first taking into account the material deposition sequence and the scanning path of the laser beam. The temperature field of the transient heat transfer analysis is then used to drive a subsequent static structural analysis. The predicted results of distortions and residual elastic strains show good correlation with the benchmark test data.

This example demonstrates the following Abaqus features and techniques:

- using temperature-dependent thermal and mechanical properties;
- performing thermomechanical simulation of additive manufacturing processes, including techniques of progressive element activation, progressive heating by a moving nonuniform heat flux, and progressive cooling on evolving free surfaces; and
- using special-purpose techniques for additive manufacturing.

This page discusses:

Products: Abaqus/Standard

Application description

Additive manufacturing (AM) technology has revolutionized design and manufacturing. Laser powder bed fusion (LPBF) is one of the common additive manufacturing technologies. During laser powder bed fusion, the recoater first deposits a thin layer of material powder, and then the laser beam scans along a predefined path acting as a heat source to melt and bind the powdered material into a solid structure. This process is repeated until the desired three-dimensional part is printed layer by layer.

Geometry

As shown in Figure 1, the bridge structure is 75 mm long, 5 mm wide, and 12 mm tall, with twelve legs that are of three different sizes. The bridge is positioned on a build plate. The length, width, and height of the build plate are 90mm, 15mm, and 12.7 mm, respectively.

Laser scan strategy and parameters

For each layer, a contour scan is followed by an infill scan. The contour scan laser travels at a speed of 900 mm/s using a power of 100 W. The infill scan laser has a speed of 800 mm/s and a power of 195 W. The laser diameters for both contour and infill are 50 μm. For odd-numbered layers, the infill scans are horizontal lines (parallel to the *X*-axis) that are separated by 0.1 mm (hatch spacing), as shown in Figure 2. For even-numbered layers, the infill scans are vertical lines (parallel to the *Y*-axis) that are also separated by 0.1 mm, as shown in Figure 3.

Recoater parameters

The recoating blade spreads powder across the powder bed surface at a speed of 80 mm/s. Each powder layer is 0.02 mm thick, and a total of 625 layers is needed to build the bridge structure. The average printing time for each layer in the legs (z=0.02 mm to z=5.00 mm) is 52 s.

Abaqus modeling approaches and simulation techniques

Abaqus/Standard provides a general framework for modeling common additive manufacturing processes, such as laser powder bed fusion. At the core of the Abaqus additive manufacturing technology is the toolpath-mesh intersection module—a powerful geometry-based engine that takes process toolpath data as input and intersects it with an arbitrary mesh. The time-location history of both material deposition sequence (recoater motion) and heating source (laser beam scanning path) can be represented by an event series in the form of a table of time, spatial coordinates, and process parameters. The toolpath-mesh intersection module takes the event series data and automatically computes all of the information required to activate elements and apply the proper thermal energy to the model. Table collections that encapsulate parameter tables or property tables can be used to define additional process parameters needed for the simulation.

The analyses in this example use the streamlined solution for powder bed–type additive manufacturing processes in Abaqus/Standard (see Thermomechanical Analysis of Powder Bed–Type Additive Manufacturing Processes Using the Trajectory-Based Method).

Progressive element activation

The toolpath-mesh intersection module uses the current position of the recoater and the finite element mesh of the bridge structure to compute which elements are active at any given time. These elements are included in a specific progressive element activation definition so that they can be activated in the required time increment. Full activation is used in this analysis. When an element is activated, its volume fraction is set to one. (See Progressive Element Activation.)

Progressive heating

The energy deposition into the system is computed by taking into account the actual path of the heat source. The toolpath-mesh intersection module provides the information pertaining to the energy deposition. The laser heat source can be modeled as a concentrated moving heat flux. (See Specifying a Concentrated Moving Heat SourceF.)

Progressive cooling

In an additive manufacturing process, radiation and convection cooling take place on the continuously evolving free surfaces. Abaqus keeps track of the free surfaces that reflect the current shape of the build part. Film or radiation conditions can be applied to the facet area of an element during progressive element activation. (See Specifying Element-Based Film Conditions on Evolving Faces of an Element in Abaqus/Standard and Specifying Element-Based Radiation Conditions on Evolving Faces of an Element in Abaqus/Standard.)

Heat transfer analysis

A transient heat transfer analysis is first performed to obtain the temperature distribution during the build process. The total step time includes the addition of 600 seconds of cooling time after the last heating event defined by the laser event series.

Mesh design

The mesh of the bridge structure consists of 8-node linear diffusive heat transfer DC3D8 elements. The elements vary in size but have a common characteristic height of 0.2 mm so that there are approximately ten layers of material in each element. The build plate is more coarsely meshed with DC3D8 elements.

Materials

The material for both the build part and the plate is nickel-based superalloy IN625. The density is taken as 8.44×10^{-9} ton/mm^3. The liquidus temperature is 1350°C, the solidus temperature is 1290°C, and the latent heat of fusion is 272×10^9 mJ/tonne.

The temperature-dependent thermal conductivity and specific heat are shown in Table 1 (source: http://www.specialmetals.com/assets/smc/documents/alloys/inconel/inconel-alloy-625.pdf).

The Stefan-Boltzmann constant is taken as 5.67×10^{-11} mW/(mm^2·K^4). The absolute zero is set at −273.15°C. The film coefficient is 0.018 mW/(mm^2·°C). For radiation heat transfer, the emissivity is 0.45.

Initial conditions

An initial temperature of 80°C is applied to the build plate. The initial temperature of the build part is 40°C, which corresponds to the temperature of the powder material as it is spread from the powder bed reservoir.

Loads

The bottom of the build tray is held at a constant 80°C. Film and radiation conditions are applied to the evolving free surfaces during the build process. The reference ambient temperature is taken to be 40°C. The table collection `ABQ_AM.Moving Heat Flux.1` referenced from the distributed flux loading defines the laser as a moving heat source.

Constraints

The connection between the bottom surface of the bridge and the top surface of the build plate is modeled as a tie constraint with the top surface of the plate as the main surface.

Output requests

Nodal temperature (NT) is requested at time points corresponding to each layer's build time.

Structural analysis

Mesh design

Full-integration solid C3D8 elements are used for both the bridge and the build plate, maintaining the same mesh topology used in the heat transfer analysis.

Materials

The temperature-dependent coefficient of thermal expansion, elastic modulus, and Poisson's ratio are shown in Table 1. Orthotropic plasticity with hardening is used. The material's yield stress is 725 MPa in the horizontal *x*- and *y*-directions and 615 MPa in the vertical *z*-direction. The stress ratio, R_{33}, is 0.8483. The stress corresponding to a plastic strain of 0.35 is 990 MPa in the horizontal directions, and the stress in the vertical direction is scaled with the same stress ratio as that used for the yield stress (source: http://www.eos.info/material_m/werkstoffe/download/NickelAlloy_IN625.pdf).

Initial conditions

In the structural analysis the initial temperature of the build part represents a relaxation temperature (not room temperature) above which thermal straining induces negligible thermal stress (see Controlling the Scale of the Simulation and the Solution Fidelity). Upon material activation, it represents the temperature from which the initial

thermal contraction occurs. In this analysis the initial temperature of the bridge is set to 750°C. The initial temperature for the build plate is 80°C.

Boundary conditions

The bottom of the build plate is fixed in all degrees of freedoms.

Predefined fields

The thermal results for each increment during the previous transient heat transfer analysis are applied to the structural analysis as predefined fields. Abaqus automatically maps the nodal values of temperature by interpolation (both in space and time) of the previous results.

Constraints

Similar to the heat transfer analysis, a tie constraint is used to model the connection between the bottom surface of the bridge and the top surface of the build plate, with the top surface of the plate as the main surface.

Output requests

Nodal displacement (U) and displacement measured from the time the node is activated (UACT) are requested at time points corresponding to the build time of every eighth layer to reduce the size of the output database. Stress (S) and elastic strain (EE) are requested at the end of printing and after cutting. You can also request logarithmic strain (LE), plastic strain (PE), equivalent plastic strain (PEEQ), and the volume fraction of the material in the current element (EACTIVE).

Discussion of results and comparison of cases

In the physical test the part is cut via wire electron discharge machining (EDM) such that only the end portion of the part remains attached to the plate. In the simulation the cut process is modeled in a separate step with the model change feature to remove a layer of elements near the bottom of the legs. The cut section of the part deflects upward from relaxation of the as-built residual stresses.

Distortion

The distortion values are measured by the difference of the vertical deflection after and before the cut for the top of 11 ridges along the center plane. Thus, $\delta_i = z_i^{after} - z_i^{before}$, where δ_i is the vertical deflection of edge *i*. The distortions along the path are shown in Figure 4. The solid blue curve is the simulation result, and the dashed red curve is the benchmark test data.

Residual elastic strain

Residual elastic strain contour plots within the as-built bridge structure are generated and compared with the x-ray diffraction measurements results. Figure 5 and Figure 6 (https://www.nist.gov/ambench/results-chal-amb2018-01-rs-part-residual-strains) show the simulation results and benchmark test results of the elastic strain in the *x*-direction. The simulation results and benchmark test results of the elastic strain in the *z*-direction are shown in Figure 7 and Figure 8 (https://www.nist.gov/ambench/results-chal-amb2018-01-rs-part-residual-strains). Figure 9 and Figure 10 show the comparison between x-ray diffraction measurements and simulation results of the strain in the *z*-direction along the z=10.75 mm and z=2.75 mm paths in the center plane. Good correlation is found between the simulation results and the benchmark test data.

Acknowledgements

SIMULIA gratefully acknowledges TWI Ltd for their collaboration in developing this model and the National Institute of Standards and Technology for creating the Additive Manufacturing benchmark test series.

Figure 1, Figure 2, and Figure 3 are provided courtesy of the NIST website (https://www.nist.gov/ambench/amb2018-01-description).

Figure 6 and Figure 8 are provided courtesy of the NIST website (https://www.nist.gov/ambench/results-chal-amb2018-01-rs-part-residual-strains).

Input files

am_bridge_thermal_analysis.inp

Heat transfer analysis.

am_bridge_structural_analysis.inp

Static structural analysis.

The following input files contain definitions or data included in the input files listed above:

ABQ_am_special_purpose_types.inp

Types of property tables, parameter tables, and event series used by the special-purpose techniques for the simulation of common additive manufacturing processes in Abaqus.

node_bridge_part.inp

Node definitions of the bridge structure.

elem_bridge_part.inp

Element definitions of the bridge structure.

node_bridge_substrate.inp

Node definitions of the build plate.

elem_bridge_substrate.inp

Element definitions of the build plate.

es_bridge_roller.inp

Event series data of the roller motion.

es_bridge_laser.inp

Event series data of the laser scanning path.

References

https://www.nist.gov/ambench/amb2018-01-description
https://www.nist.gov/ambench/benchmark-test-data
http://www.specialmetals.com/assets/smc/documents/alloys/inconel/inconel-alloy-625.pdf
http://www.eos.info/material_m/werkstoffe/download/NickelAlloy_IN625.pdf

Tables

Table 1. Temperature-dependent material properties of IN625.

Temperature	Thermal Conductivity (mW/(mm·°C))	Specific Heat (mJ/(tonne·°C))	Coefficient of Thermal Expansion (1/°C)	Elastic Modulus (MPa)	Poisson's Ratio
21 °C	9.8	4.1×10^8	–	2.075×10^5	0.278

Temperature	Thermal Conductivity (mW/(mm·°C))	Specific Heat (mJ/(tonne·°C))	Coefficient of Thermal Expansion (1/°C)	Elastic Modulus (MPa)	Poisson's Ratio
93 °C	10.8	4.27×10^{8}	1.28×10^{-5}	2.041×10^{5}	0.28
204 °C	12.5	4.56×10^{8}	1.31×10^{-5}	1.979×10^{5}	0.286
316 °C	14.1	4.81×10^{8}	1.33×10^{-5}	1.917×10^{5}	0.29
427 °C	15.7	5.11×10^{8}	1.37×10^{-5}	1.855×10^{5}	0.295
538 °C	17.5	5.36×10^{8}	1.4×10^{-5}	1.786×10^{5}	0.305
649 °C	19	5.65×10^{8}	1.48×10^{-5}	1.703×10^{5}	0.321
760 °C	20.8	5.9×10^{8}	1.53×10^{-5}	1.606×10^{5}	0.34
871 °C	22.8	6.2×10^{8}	1.58×10^{-5}	1.475×10^{5}	0.336
927 °C	–	–	1.62×10^{-5}	–	–
982 °C	25.2	6.45×10^{8}	–	–	–
1093 °C	–	6.7×10^{8}	–	–	–

Figures

Figure 1. Schematic of the bridge structure as given by NIST.

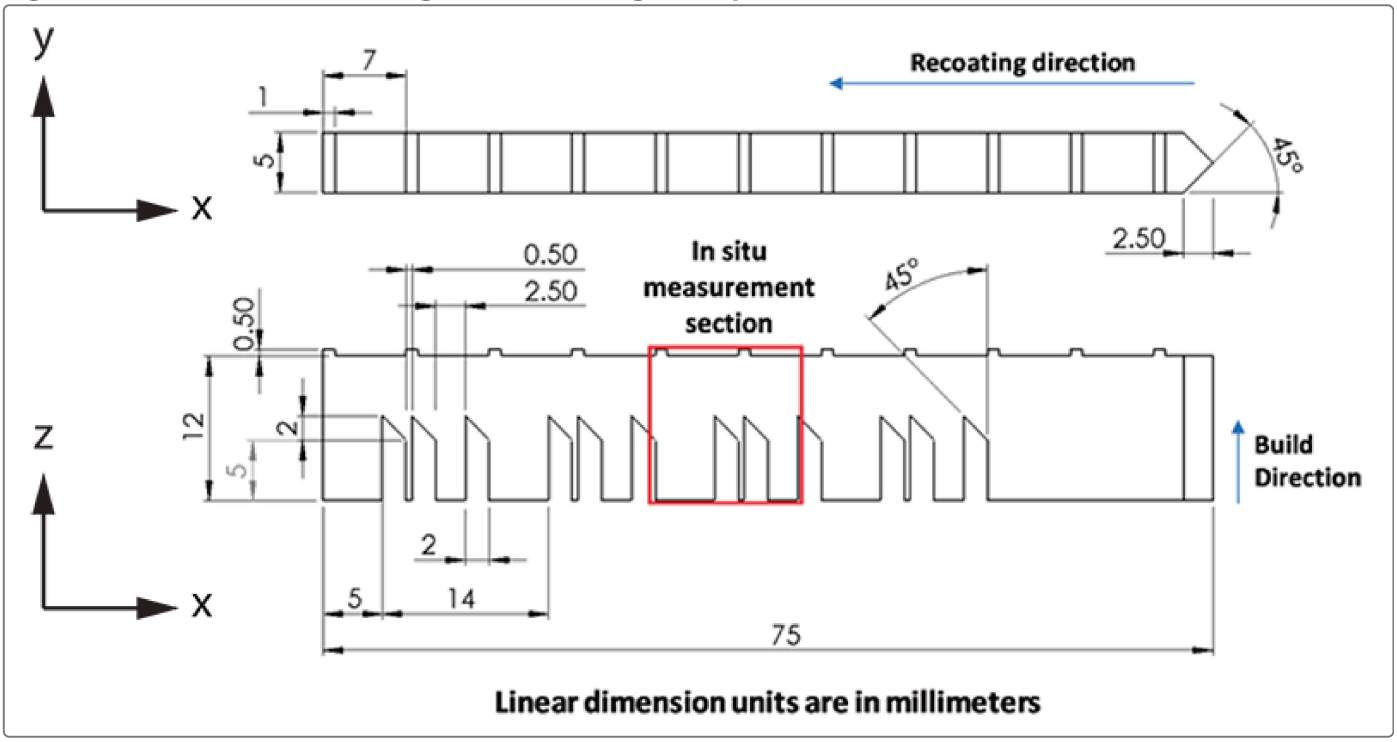

Figure 2. Odd-numbered layer scan strategy as given by NIST.

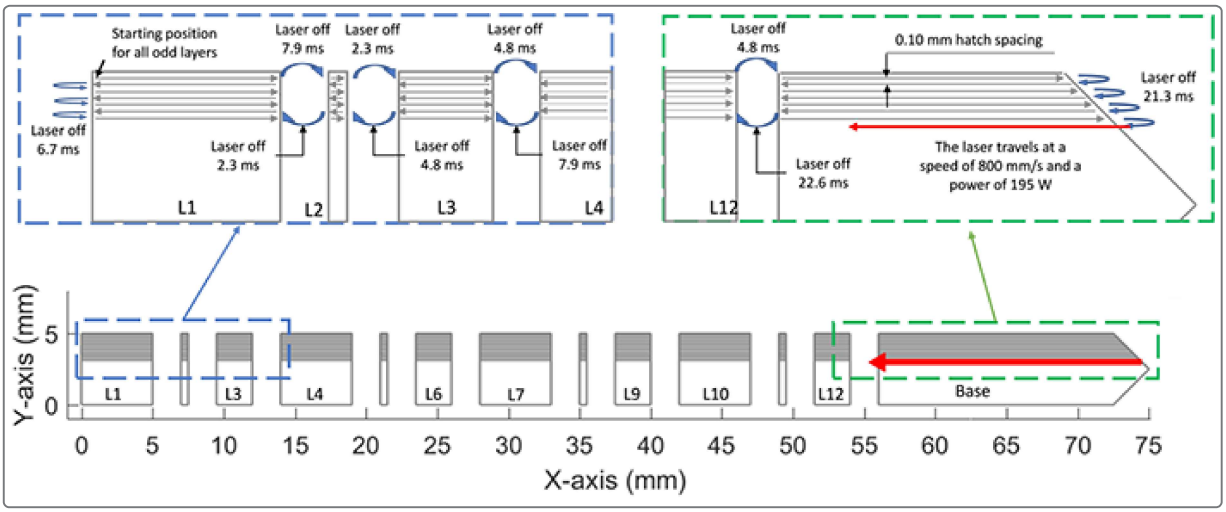

Figure 3. Even-numbered layer scan strategy as given by NIST.

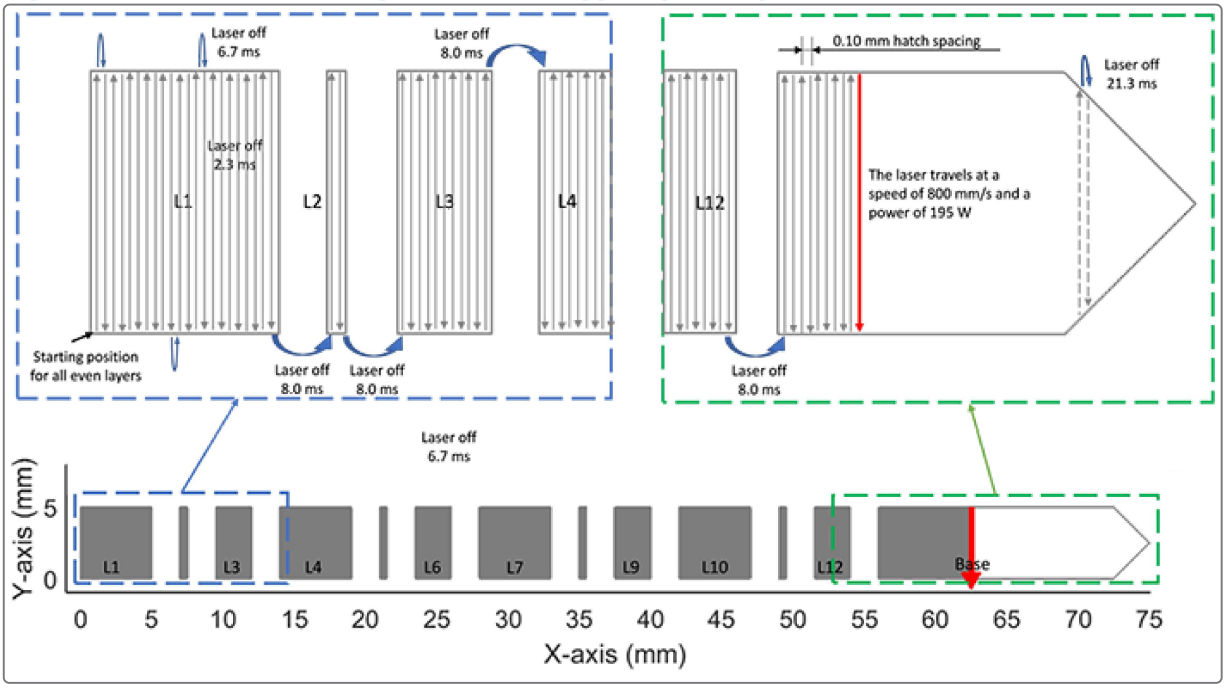

Figure 4. Upward deflection of the top of 11 ridges in the center plane.

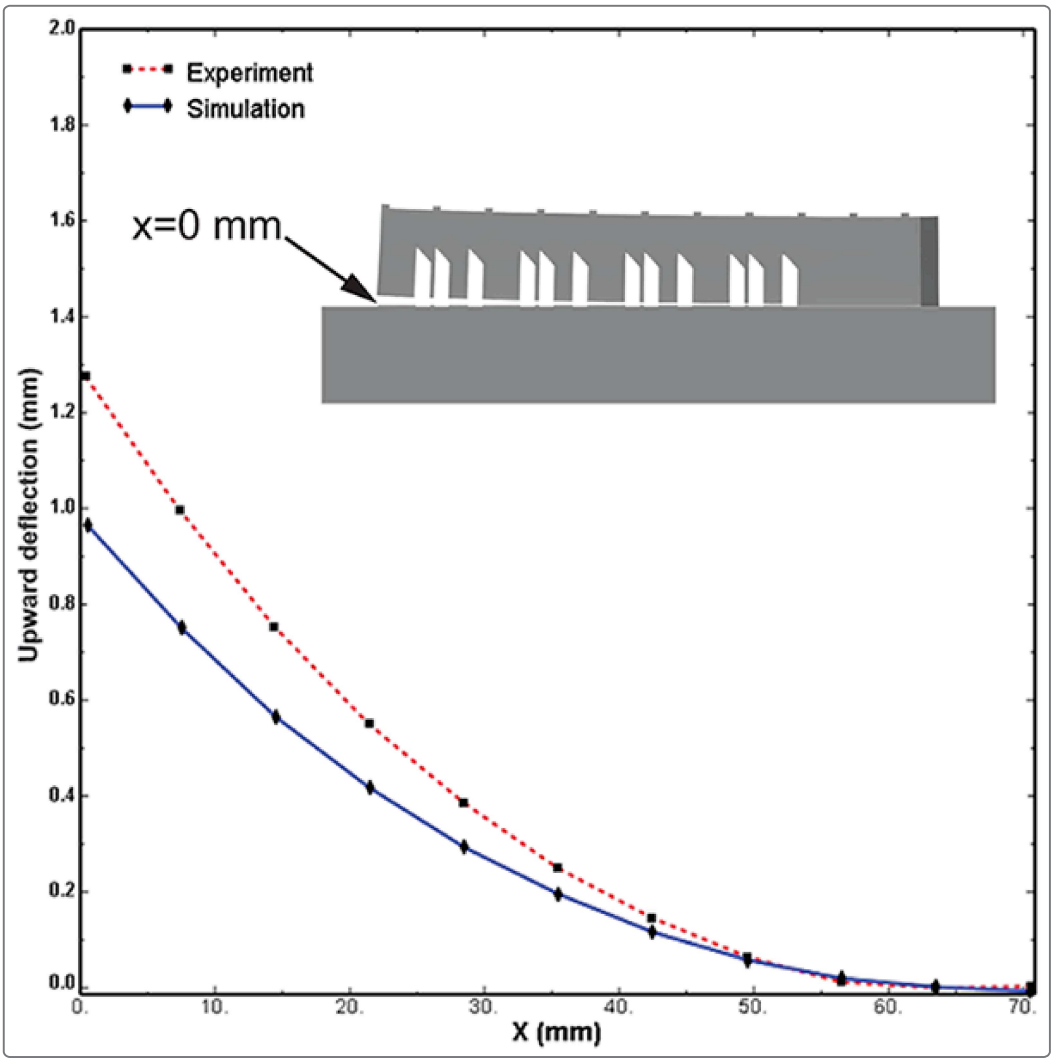

Figure 5. Simulation result of elastic strain in the *x*-direction.

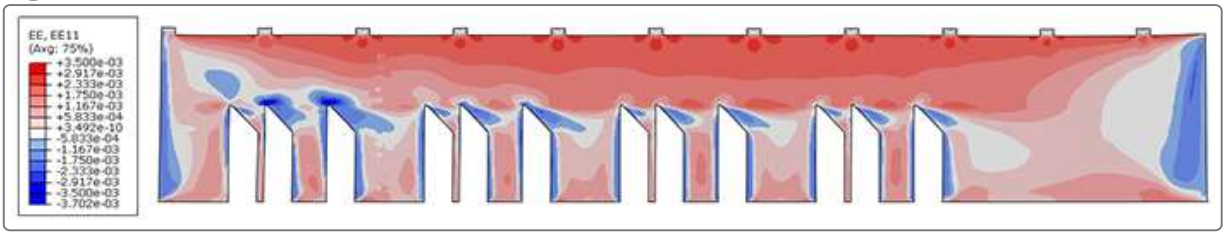

Figure 6. X-ray diffraction measurement of elastic strain in the *x*-direction as published by NIST.

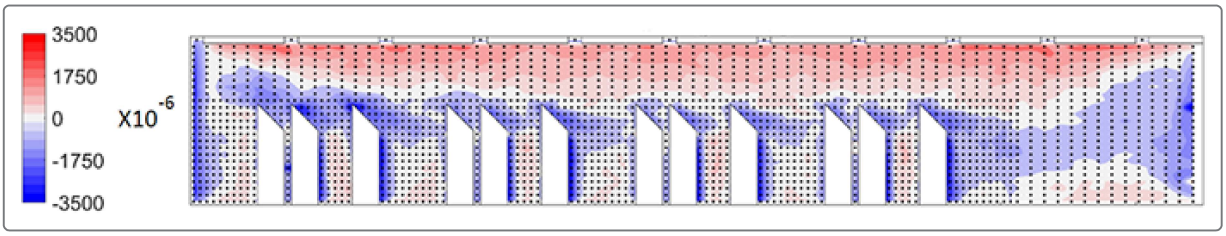

Figure 7. Simulation result of elastic strain in the *z*-direction.

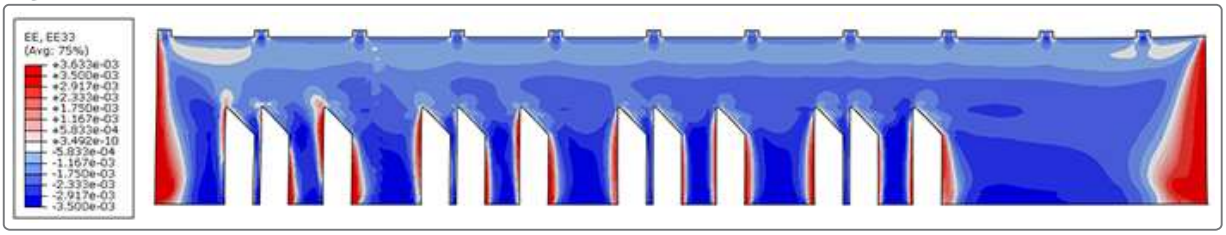

Figure 8. X-ray diffraction measurement of elastic strain in the *z*-direction as published by NIST.

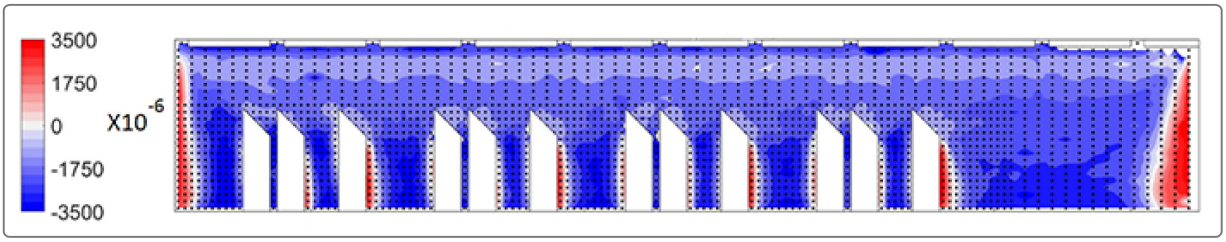

Figure 9. X-ray diffraction measurement and simulation result of elastic strain in the *z*-direction along the *z*=10.75 mm path.

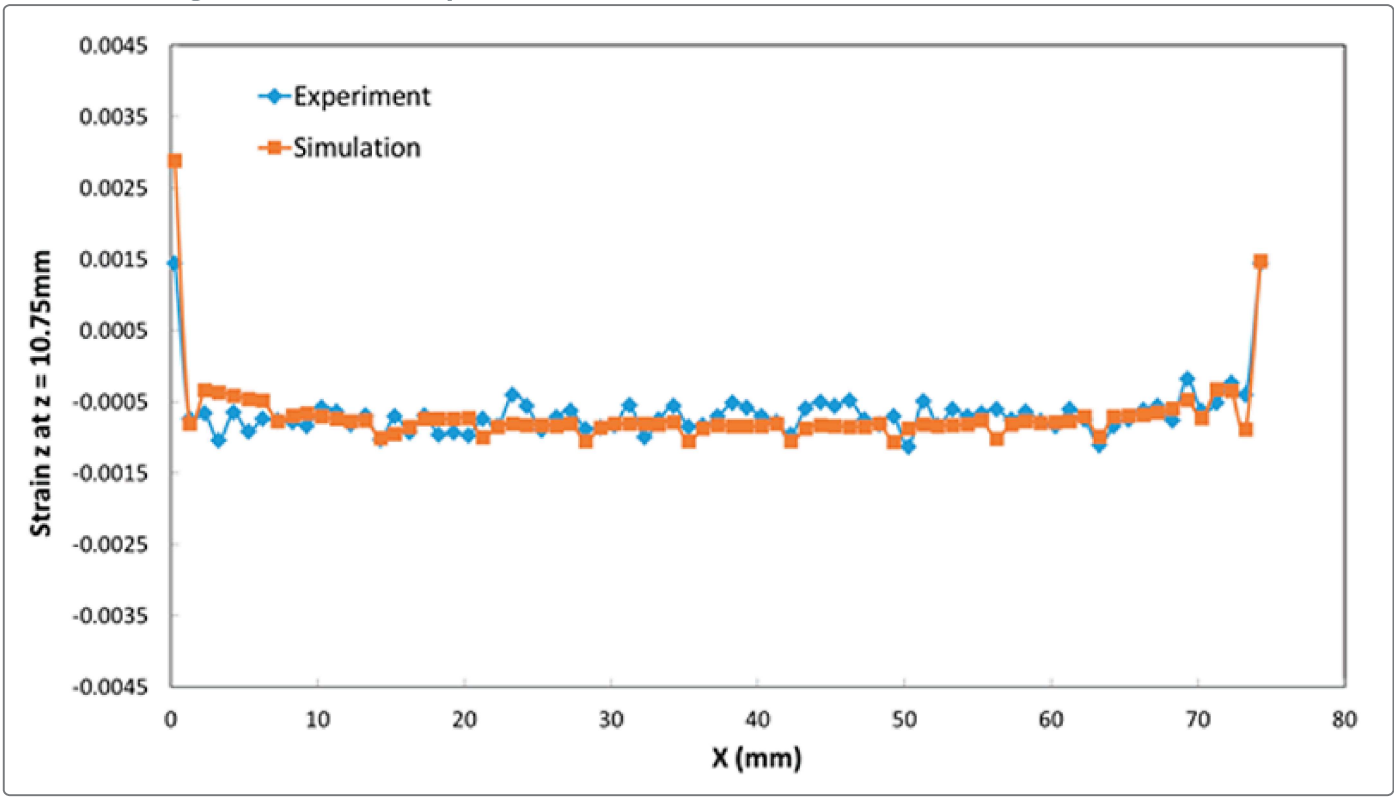

Figure 10. X-ray diffraction measurement and simulation result of elastic strain in the *z*-direction along the *z*=2.75 mm path.

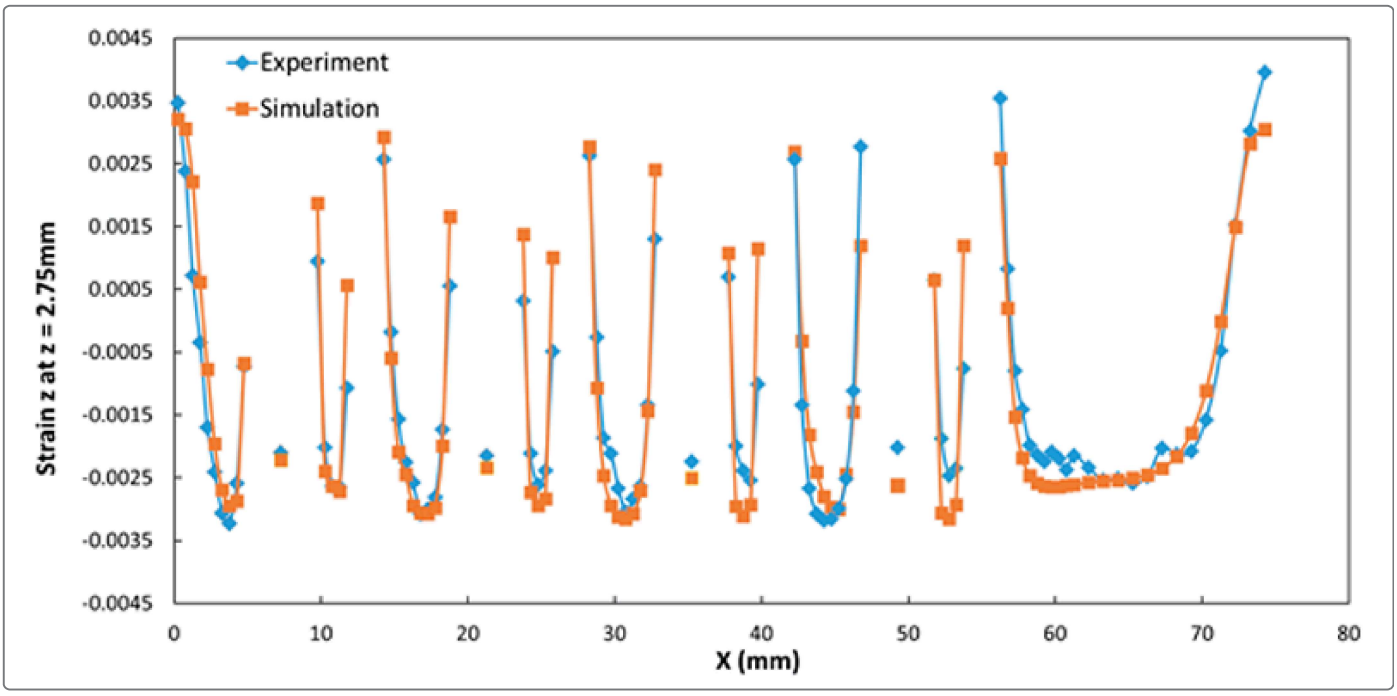
Experiment
Simulation
Strain z at z = 2.75mm
X (mm)
0.0045
0.0035
0.0025
0.0015
0.0005
-0.0005
-0.0015
-0.0025
-0.0035
-0.0045
0
10
20
30
40
50
60
70
80